Available online at www.sciencedirect.com
ScienceDirect
Ceramics International 34 (2008) 1609–1615
CERAMICS INTERNATIONAL
www.elsevier.com/locate/ceramint

Pressureless sintered Al_2O_3–SiC nanocomposites

S. Gustafsson [a], L.K.L. Falk [a,*], E. Lidén [b], E. Carlström [b]

[a] *Department of Applied Physics, Chalmers University of Technology, SE-412 96 Göteborg, Sweden*
[b] *Swedish Ceramic Institute, SE-431 53 Mölndal, Sweden*

Received 12 January 2007; accepted 19 April 2007
Available online 15 June 2007

Abstract

Al_2O_3 + 5 vol% SiC composite ceramics were prepared via a conventional powder processing route followed by pressureless sintering. Commercially available Al_2O_3 and SiC powders were milled together in an aqueous suspension. The slurry was freeze granulated, and green bodies were obtained by cold isostatic pressing of the granules. Pressureless sintering was carried out in a nitrogen atmosphere at 1750 and 1780 °C. Near full density (>99%) was achieved at 1780 °C. Densification at the lower sintering temperature was promoted by smaller additions of MgO. Vickers hardness and indentation fracture toughness varied around 18 GPa and 2.3 MPa $m^{1/2}$ after sintering at 1780 °C. Transmission electron microscopy revealed that the SiC particles were located predominantly to the interior of the matrix grains and well distributed throughout the composite microstructures. The intragranular particles had sizes in the range 50–200 nm while the intergranular particles were larger, typically 200–500 nm in diameter.
© 2007 Elsevier Ltd and Techna Group S.r.l. All rights reserved.

Keywords: B. Nanocomposites; B. Electron microscopy; D. Al_2O_3; D. SiC; Pressureless sintering

1. Introduction

The nanocomposite approach to engineered ceramic microstructures has received much attention in the ceramic literature [1–8]. This research area was initiated by Niihara who reported large improvements in the mechanical properties when a ceramic material was reinforced with nanometer sized particles [1]. There has, however, been a wide spread in the results presented by different researchers because of differences in fabrication and testing procedures, and some of the improvements have not been reproduced.

The production of a fully dense material with a homogeneous dispersion of the reinforcing agent is a key factor in the fabrication of ceramic nanocomposites. A porous microstructure and agglomerated second phase particles would degrade the performance of the composite material [3,5,6,9]. It is well established that inclusions of second phase particles may suppress grain growth, but the particles will also obstruct densification [1,2,4,6,10]. A composite ceramic may, therefore, require a higher sintering temperature than the monolithic material. In addition, it may be necessary to apply an external pressure during densification in order to achieve a sufficiently high density. Hot pressing has, hence, generally been used for the fabrication of dense ceramic nanocomposite materials [1,6,8]. Hot pressing is, however, costly, and does also put restrictions on the sample geometry. Pressureless sintering is, from this point of view, an interesting alternative for the densification of composite green bodies. Pressureless sintered Al_2O_3–SiC composites have previously in general been fabricated with smaller additions of MgO [11–13], or the addition of ~1 wt% or more of other metal oxides [12–14].

This paper presents a fabrication process for high density pressureless sintered Al_2O_3–5 vol% SiC nanocomposites without additives. Composites with smaller additions (0.1 wt% or less) of MgO were also fabricated as reference materials. The resulting microstructures were examined in the scanning and transmission electron microscopes (SEM and TEM), and particular attention was paid to the matrix grain size, and the size and location of the SiC particles. Vickers hardness and indentation fracture toughness were also determined, and related to the microstructural properties.

* Corresponding author.
E-mail address: lklfalk@fy.chalmers.se (L.K.L. Falk).

0272-8842/$34.00 © 2007 Elsevier Ltd and Techna Group S.r.l. All rights reserved.
doi:10.1016/j.ceramint.2007.05.005

2. Experimental procedures

2.1. Materials

A powder mixture of Al_2O_3 (AKP 30, Sumitomo, Japan; mean particle size 0.4 μm) and 4.1 wt% SiC (UF 25, H.C. Starck, Germany; mean particle size 0.45 μm; 2.5 wt% oxygen) was milled in water for 1.5 h with Si_3N_4 balls. The aqueous suspension had a solid loading of 40 vol%, and contained a dispersant (Dolapix PC 21; 0.35 wt% with respect to the Al_2O_3 and SiC contents). Two doped suspensions were also prepared by adding MgO (0.05 and 0.1 wt% with respect to the Al_2O_3 content) after 1 h of milling. The Al_2O_3:SiC powder weight ratio was chosen so that the sintered material would have a SiC volume fraction of 5%. The experimental materials are shown in Table 1.

After milling, the slurries were screened through a 50 μm mesh, and a pressing aid (PEG 400; 3 wt% with respect to the Al_2O_3 and SiC contents) was added. The slurries were then stirred for 1 h, and thereafter screened through a 100 μm mesh. Freeze granulation was subsequently carried out by spraying into liquid nitrogen. The ice was removed by freeze drying and the granules were screened so that the fraction larger than 500 μm was removed. Freeze granulation and drying makes it possible to retain the homogeneity of the aqueous suspension in the ceramic green bodies [15].

The granules were hand-pressed into compacts and these were cold isostatically pressed at 300 MPa. The green bodies were placed in a SiC protective powder bed in a graphite crucible and pressureless sintered in a nitrogen atmosphere for 4 h. Two different sintering temperatures, 1750 and 1780 °C, were applied (see Table 1). The heating rate of the furnace was 1 °C/min up to 600 °C, and then 10 °C/min up to the holding temperature. The density of the sintered material was determined by the Archimedean method using distilled water.

2.2. Electron microscopy

The overall structures of the sintered materials were investigated in the SEM (Leo ULTRA 55). Specimens for SEM were polished to a 1 μm surface finish using diamond spray, and thereafter thermally etched for 15 min at 1300 °C in an argon atmosphere. In order to avoid charging effects under the electron beam in the SEM, a thin layer of carbon was deposited on the specimen surface. Grain size measurements were performed on the alumina matrix using the mean linear intercept method. An average matrix grain size was determined by multiplying the mean value of the linear intercept measurements by 1.5. At least 400 intercepts were determined for each material.

TEM thin-foil specimens were prepared from thin slices ground to a thickness of around 100 μm and polished to a surface finish of 3 μm using diamond spray. Discs, 3 mm in diameter, were cut by an ultrasonic drill, dimpled and finally ion-thinned to electron transparency. A thin layer of carbon was evaporated onto one side of the thin-foils in order to avoid charging effects during imaging and analysis in the TEM (Philips CM200 FEG-TEM). SiC particles were identified by energy dispersive X-ray analysis (EDX; Link ISIS system) in combination with energy filtered TEM (Gatan imaging filter, GIF). Combined analytical and spatial information was obtained from images recorded around the carbon K, oxygen K and aluminium $L_{2,3}$ edges in the electron energy loss spectrum (EELS). An energy selecting slit width of 20 eV was used for the acquisition of the pre- and post-edge images around the aluminium $L_{2,3}$ edge, while 30 and 40 eV slits were used for the pre- and post-edge images around the carbon K and oxygen K edges, respectively. Elemental distribution images were displayed as the jump ratio between a post- and a pre-edge image. A brighter contrast in the calculated images reflects a higher concentration of the particular element.

The SiC particle size distributions in the undoped material and the material with an addition of 0.05 wt% MgO were estimated after sintering at the two temperatures. Around 300–400 particles were measured in TEM micrographs of randomly selected areas of the microstructures.

2.3. Mechanical testing

Hardness and indentation fracture toughness were determined from Vickers impression marks. Approximately, the outer 2 mm of a sintered sample was removed with a low speed saw. The sample was then ground flat, and the surface was polished to a 1 μm finish using diamond spray.

Vickers indents were made with a load of 98.1 N (10 kg) and an impression time of 30 s. The Vickers hardness (H) was calculated according to:

$$H = 1.8544\frac{P}{d^2} \quad (1)$$

where P is the load and d is the length of the impression diagonal. The indentation fracture toughness was determined

Table 1
The experimental materials

Material	Sintering temperature (°C)	Density (%)	Matrix grain size (μm)	Fraction measured SiC particles <200 nm (%)	Hardness (GPa)	K_{1C} (MPa $m^{1/2}$)
Al_2O_3–SiC	1750	93.9	2.4	80	14.1	2.4
Al_2O_3–SiC (+0.05 wt% MgO)	1750	96.2	2.3	82	15.2	2.3
Al_2O_3–SiC (+0.1 wt% MgO)	1750	97.9	2.6		16.8	2.3
Al_2O_3–SiC	1780	98.9	3.1	85	18.3	2.4
Al_2O_3–SiC (+0.05 wt% MgO)	1780	99.3	3.1	74	18.0	2.3
Al_2O_3–SiC (+0.1 wt% MgO)	1780	99.3	3.2		17.4	2.3

according to Anstis equation [16]:

$$K_{IC} = 1.6 \times 10^{-2} \left(\frac{E}{H}\right)^{1/2} \left(\frac{P}{c_0^{3/2}}\right) \quad (2)$$

where E is Young's modulus, H the Vickers hardness and c_0 is half the crack diagonal. A value of Young's modulus for the nanocomposite was calculated to 381.7 MPa using the rule of mixture with $E(Al_2O_3) = 380$ MPa and $E(SiC) = 414$ MPa. Both d and c_0 in Eqs. (1) and (2) were measured on SEM secondary electron images.

3. Results

3.1. Matrix microstructure

There was a pronounced effect of a small MgO addition on the densification at 1750 °C (see Table 1). The two materials doped with MgO reached 96.2% (0.05 wt% MgO) and 97.9% (0.1 wt% MgO) of full density, while the undoped material only reached 93.9%. The effect of a MgO addition on density was less pronounced at the higher sintering temperature 1780 °C. The two doped materials reached 99.3%, and the undoped material 98.9%, of full density. TEM revealed that the porosity was exclusively intergranular in all microstructures, and often associated with smaller agglomerates of SiC particles (see Fig. 1).

The average matrix grain size increased at the higher sintering temperature (see Table 1). The smaller MgO additions had, however, no pronounced effect on the grain size at any of the sintering temperatures (Table 1; Fig. 2). The etched surfaces showed that the matrix grain section area distributions of both undoped and doped materials were narrow. Only a limited number of larger grain sections (up to ~10 μm in diameter) were observed in the microstructures of the materials sintered at 1780 °C.

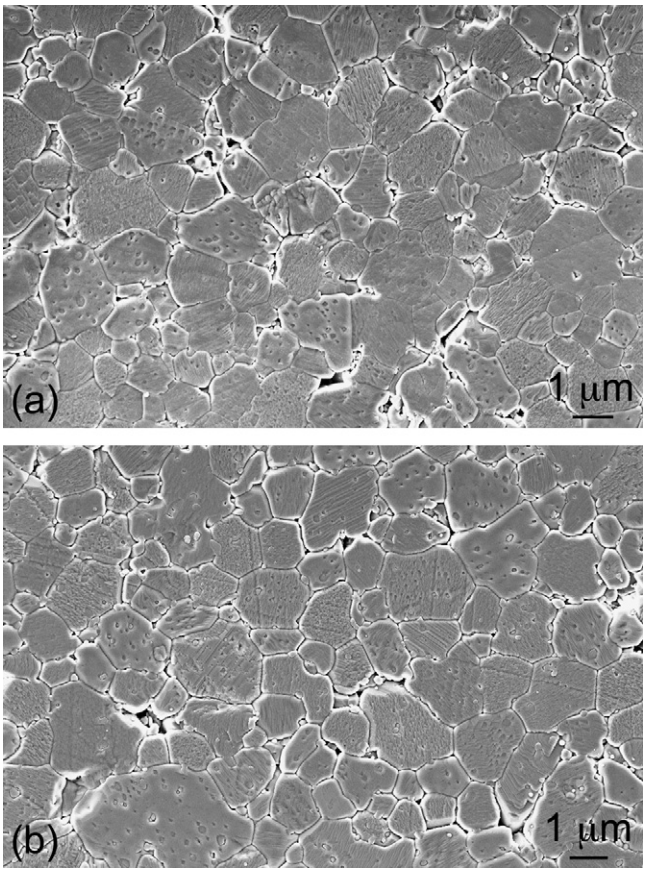

Fig. 2. Thermally etched surfaces of the materials sintered at 1780 °C: (a) without MgO and (b) with 0.05 wt% MgO.

The overall matrix dislocation density was low. Occasional dislocations were pinned by intragranular SiC particles (see Fig. 3).

Grain boundary phases were not identified in these microstructures as shown in Fig. 4.

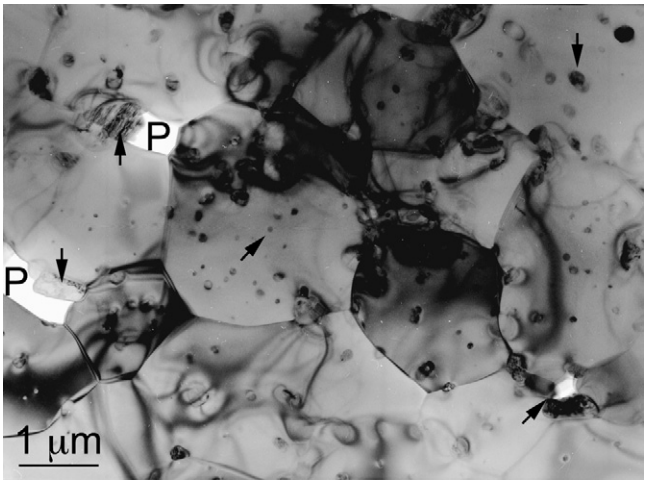

Fig. 1. Intra- and intergranular SiC particles (arrowed) in the microstructure of the material sintered at 1750 °C without MgO. Some larger particles were associated with intragranular pores (P).

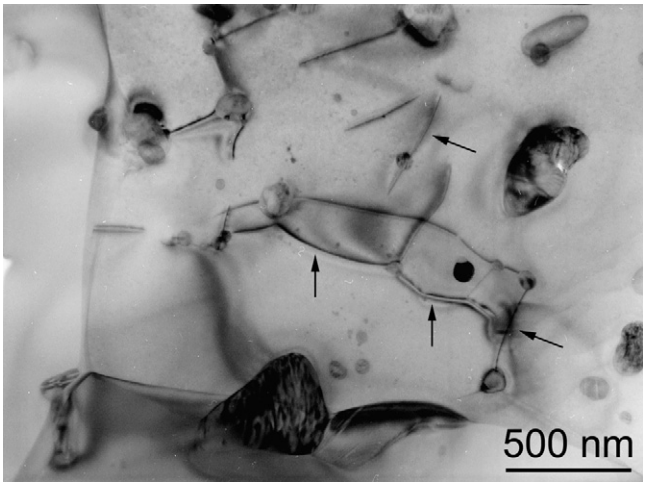

Fig. 3. Dislocations (arrowed) pinned by, or emerging from, SiC particles inside a matrix grain in the material sintered at 1750 °C with the addition of 0.05 wt% MgO.

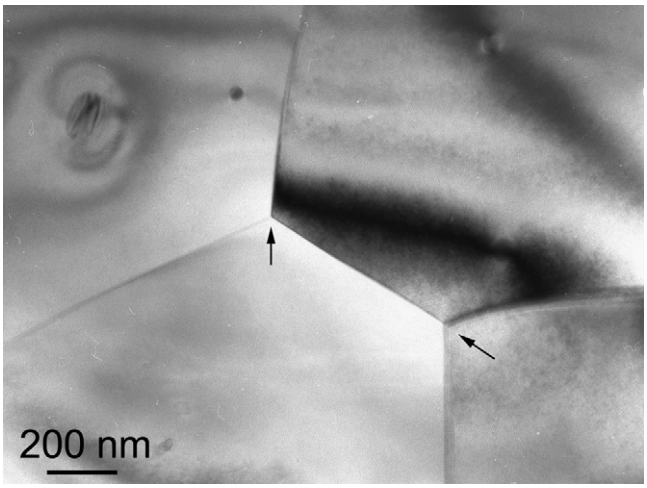

Fig. 4. Grain boundaries and triple grain junctions (arrowed) in the material sintered with 0.1 wt% MgO at 1780 °C.

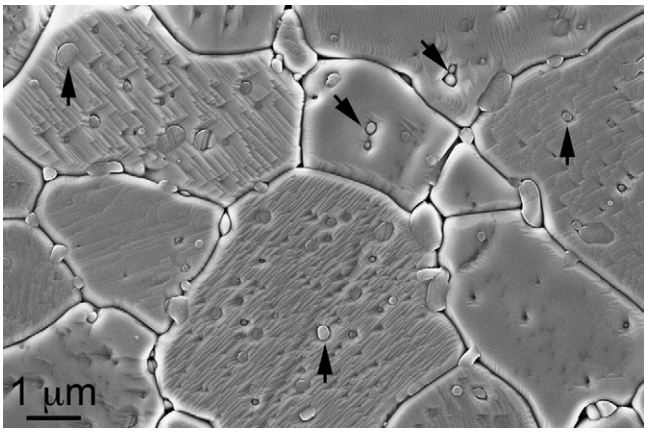

Fig. 6. Thermally etched surface of the material sintered with 0.05 wt% MgO at 1780 °C. SiC particles (arrowed) are predominantly located to intragranular positions. A smaller fraction of larger particles are present at the grain boundaries.

3.2. SiC particles

EDX point analysis and elemental distribution images computed from energy filtered images (Fig. 5) confirmed that the second phase particles were SiC. The SiC particles were well dispersed in the microstructures, and located predominantly to the interiors of the Al_2O_3 matrix grains (see Figs. 6 and 7). Only a smaller fraction of larger particles (200–500 nm) were present at grain boundaries. Imaging in the TEM showed that strain contours were associated with the intragranular SiC particles (see Fig. 8).

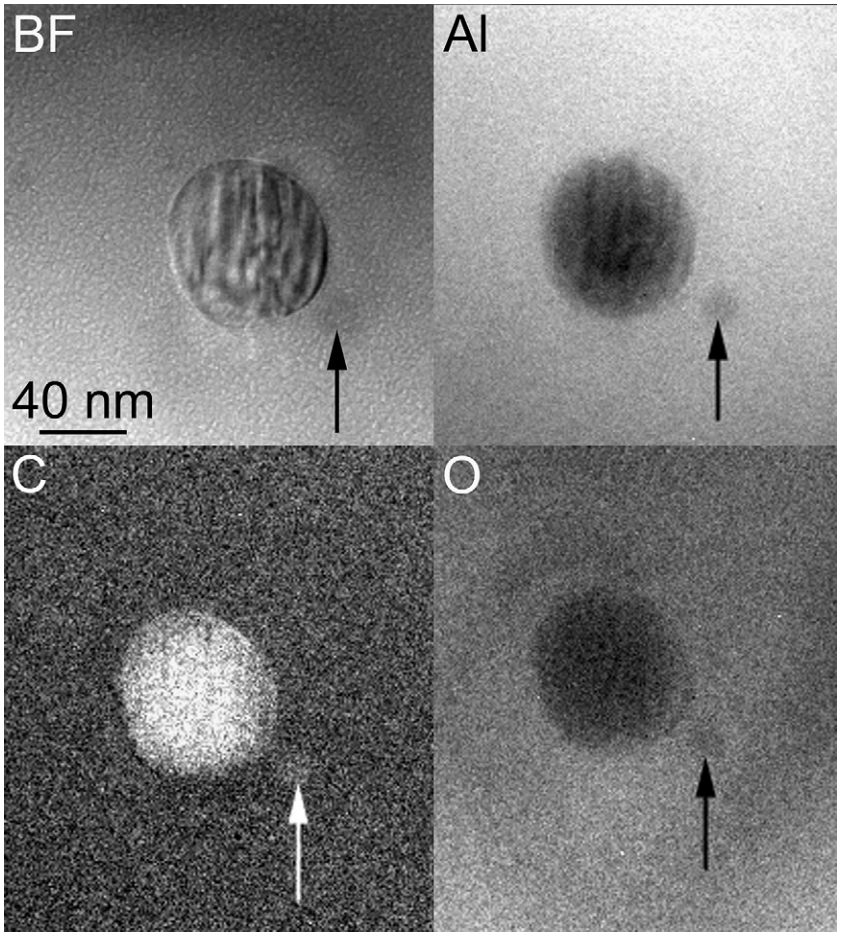

Fig. 5. Bright field image (BF) and aluminium, carbon and oxygen jump ratio images of SiC particles in the material sintered at 1780 °C without the addition of MgO. Note the small (∼20 nm) SiC particle (arrowed).

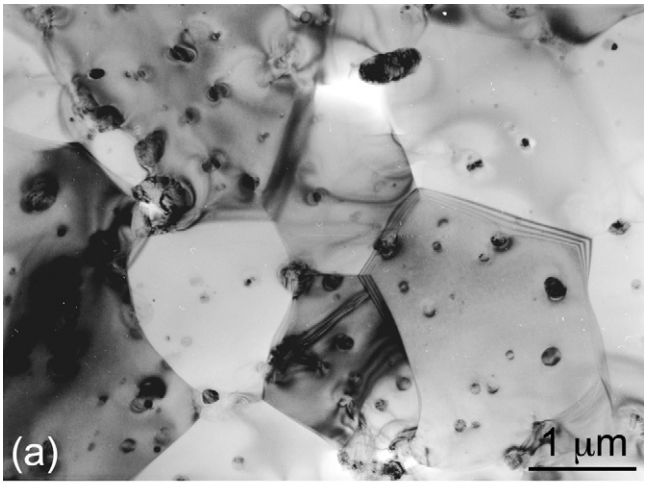

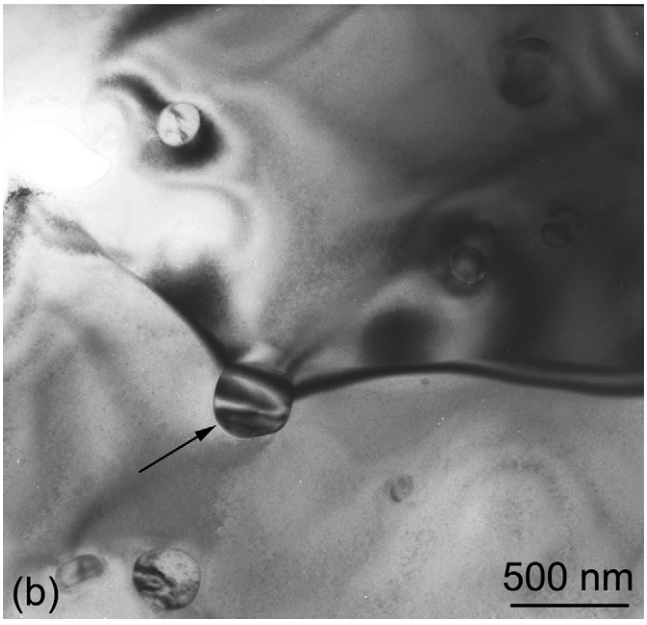

Fig. 7. (a) Well dispersed SiC particles at inter- and intragranular positions in the material sintered at 1750 °C without MgO. (b) Grain boundary pinning by a SiC particle (arrowed) in the material sintered at 1780 °C with the addition of 0.1 wt% MgO.

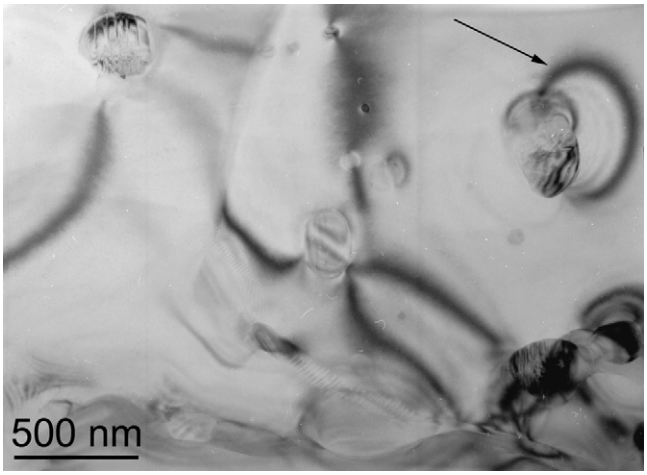

Fig. 8. Strain contours (arrowed) around SiC particles in the material sintered at 1780 °C without addition of MgO.

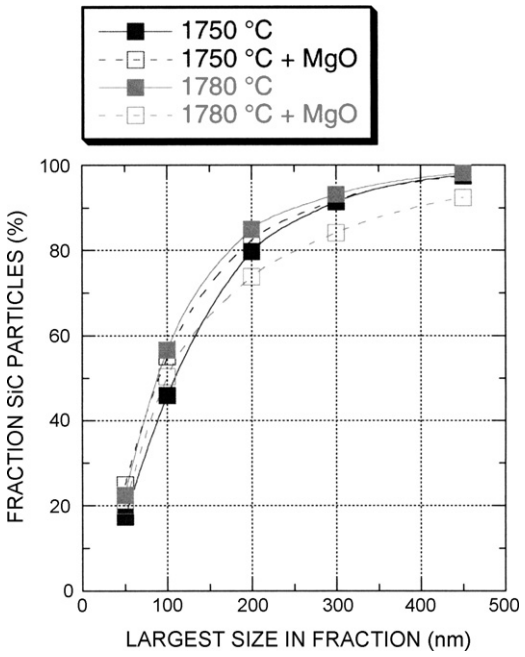

Fig. 9. Cumulative fraction of SiC particles against particle size in the materials sintered without the addition of MgO and with an addition of 0.05 wt% MgO.

The diagram in Fig. 9 shows the cumulative fraction of SiC particles against particle size in the materials sintered without the addition of MgO or with an addition of 0.05 wt% MgO. Around 80% of the particles in the four microstructures had sizes <200 nm (see Table 1; Fig. 9). The four curves have similar shapes, although the curve for the SiC particles in the material sintered with 0.5 wt% MgO at 1780 °C falls slightly below the other three when the largest particle size in the fraction is between 200 and 450 nm (Fig. 9).

3.3. Mechanical properties

Vickers hardness of the materials sintered at 1750 °C increased with density (see Table 1). The material without an addition of MgO had the lowest hardness, 14.1 GPa, and the addition of 0.1 wt% MgO resulted in a hardness of 16.8 GPa. The materials sintered at 1780 °C were close to fully dense, and their hardness varied between 17.4 and 18.3 GPa (see Table 1).

The indentation fracture toughness (K_{IC}) was determined to either 2.3 or 2.4 MPa $m^{1/2}$, and seemed to be independent of composition, density and matrix grain size (see Table 1). SEM indicated a predominantly transgranular fracture mode [17].

4. Discussion

The work presented in this paper demonstrates that it is possible to pressureless sinter Al_2O_3–5 vol% SiC nanocomposites to near full density without additives. A smaller addition of MgO is an effective densification aid only at lower sintering temperatures (1750 °C), while the density of doped and undoped materials are virtually the same after sintering at a higher temperature (1780 °C). The thermal energy at the higher sintering temperature is, hence, sufficient in order to activate

mechanisms of materials transport that lead to a virtually fully dense composite ceramic material without an applied pressure (see Table 1).

4.1. The addition of MgO

It is well documented that a smaller addition (a few hundred ppm) of MgO is an effective densification aid during sintering of Al_2O_3 ceramics at temperatures in the range 1600–1900 °C [18,19]. Such small additions of MgO have also been reported to control the Al_2O_3 grain size by suppressing exaggerated grain growth [18–20]. The smaller additions of MgO to the materials in the present investigation did, however, not have any obvious effect on matrix grain size during sintering at a particular temperature (see Table 1). A limited number of larger matrix grain section areas were present also in the composites sintered with a smaller addition of MgO. This indicates that local abnormal grain growth did occur under the applied sintering conditions, despite the MgO addition.

MgO may promote a more homogeneous grain size distribution by solute pinning of grain boundaries [20]. Other mechanisms that may operate in the presence of a glassy/liquid phase include modification of liquid–solid interfacial energies and glass viscosity [18]. It has been shown, however, that the concentration of MgO has to be at least as large as that of impurity phases like SiO_2 in order to hinder abnormal grain growth [12,19]. The oxygen contents of the SiC starting powder correspond to 4.7 wt% SiO_2 which is a comparatively large amount. The relative weight fractions of MgO and SiO_2 were 28 and 72 wt%, respectively, when 0.05 wt% MgO had been added. When 0.1 wt% MgO had been added, the relative fractions were 44 wt% MgO and 56 wt% SiO_2. The concentration of SiO_2 in the starting powder mixtures was, hence, in both cases significantly higher than that of MgO. This may explain the limited number of larger grain section areas observed also in the MgO containing materials.

4.2. The SiC particles

It is well established that the presence of SiC particles will impede alumina matrix grain growth [6,10]. This was observed also in these microstructures. Grain boundaries were frequently pinned by larger (a few hundred nm) SiC particles (see Fig. 7), and the pinning caused a ‘‘wavy’’ grain boundary appearance. Smaller SiC particles are generally less effective in pinning moving grain boundaries, and this fraction of the particles tend to end up at intragranular positions [1,5]. This phenomenon was observed also in this work, and is illustrated in Fig. 10, where an Al_2O_3 grain is seen to encompass a SiC particle.

The SiC particle size was significantly reduced during fabrication. The as-received SiC powder particle size distribution had $d_{50} = 0.45$ μm, while the diagram in Fig. 9 indicates a value of d_{50} of around 0.1 μm in the sintered materials. More than 90% of the SiC particles in the sintered materials were smaller than 0.45 μm (see Fig. 9). The diagram in Fig. 9 also suggests that MgO had a clear effect on the SiC particle size distribution during sintering at 1780 °C.

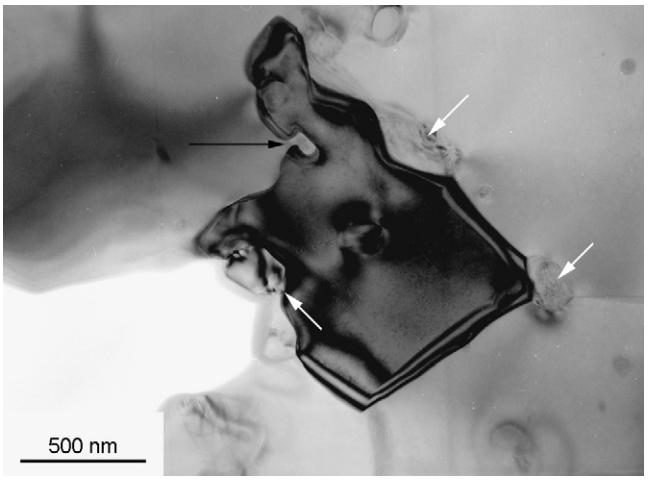

Fig. 10. An alumina grain growing around a small SiC particle (black arrow). Larger SiC particles (white arrows) remain at intergranular positions. Material sintered at 1750 °C without MgO.

The SiC particle size reduction may, in part, have been achieved during powder processing prior to freeze granulation, but also through particle refinement during sintering. The oxygen contents of the SiC starting powder correspond to a surface silica content of 4.7 wt%. This surface silica would react with the Al_2O_3 during the sintering cycle; the lowest eutectic temperature in the SiO_2–Al_2O_3 system is around 1587 °C at 5 wt% Al_2O_3 [21]. Local liquid formation would promote a solution-reprecipitation process of the SiC [22]. The diagram in Fig. 9 suggests that an addition of MgO to this liquid affects this process and the SiC particle size distribution in the sintered composite.

Strain contours, associated with the SiC particles, were observed in the matrix grains throughout these microstructures (see Fig. 8). The lattice strain giving rise to these contours would be caused by stresses induced during cooling because of the thermal expansion mismatch between the matrix and the SiC particles. The thermal expansion coefficient of Al_2O_3 ($\alpha = 8.8 \times 10^{-6}\ °C^{-1}$) is significantly higher than that of SiC ($\alpha = 4.7 \times 10^{-6}\ °C^{-1}$) [21]. Compressive average stresses in the range 1500–2000 MPa in the SiC particles and tensile average stresses of 200–700 MPa in the alumina matrix have been reported [8,23,24]. It has been suggested that the stress at the particle/matrix interface may be high enough to activate slip systems in the alumina [25,26]. Dislocations present around SiC particles (see Fig. 3) may have been introduced in that way.

4.3. The mechanical properties

The variation in the density of the composites was reflected in their hardness (see Table 1). The hardness of the nearly dense materials sintered at 1780 °C is in accordance with previous reports on Al_2O_3–5 vol% SiC materials of similar density, matrix grain size and SiC particle size [3,6].

There was no significant difference in the indentation fracture toughness between the materials (see Table 1). Values of 2.3–2.4 MPa $m^{1/2}$ are, however, slightly lower than what is generally found in the literature. Indentation fracture toughness

values between 2.5 and 4.0 MPa $m^{1/2}$ have been reported for Al_2O_3–5 vol% SiC nanocomposites [2,3,6,8]. These values were generally slightly higher than that obtained for a monolithic alumina reference material.

A transgranular fracture mode may be explained in terms of grain boundary strengthening and matrix weakening due to the thermal residual stresses that develop during cooling from the sintering temperature [1,2,6,7]. Radial compressive forces and tangential tensile forces will develop around the SiC particles since the Al_2O_3 matrix has a larger coefficient of thermal expansion than the SiC. This may lead to matrix weakening and grain boundary strengthening, thus promoting a transgranular fracture mode.

5. Concluding remarks

It is possible to pressureless sinter undoped Al_2O_3–5 vol% SiC nanocomposites to near full density (99.3%) at 1780 °C. A smaller addition of MgO (0.05 or 0.1 wt% with respect to the Al_2O_3) is an effective densification aid only at lower sintering temperatures (1750 °C), while the density of doped and un-doped materials are virtually the same after sintering at a higher temperature (1780 °C). The SiC nanoparticles are well distributed and present at predominantly intragranular positions.

The hardness is strongly dependent on the density, and in the range 17.0–18.5 GPa when the material was sintered at 1780 °C. The indentation fracture toughness was 2.3–2.4 MPa $m^{1/2}$ and did not depend on density, matrix grain size or SiC particle size.

Acknowledgements

Daniel Käck and Martin Sjöstedt are gratefully thanked for assistance in the fabrication of the materials. Financial support was received from the Swedish Foundation for Strategic Research.

References

[1] K. Niihara, New design concept of structural ceramics–ceramic nanocomposites, J. Ceram. Soc. Jpn. 99 (10) (1991) 974–982.
[2] J. Zhao, L.C. Stearns, M.P. Harmer, H.M. Chan, G.A. Miller, R.E. Cook, Mechanical behavior of alumina–silicon carbide nanocomposites, J. Am. Ceram. Soc. 76 (2) (1993) 503–510.
[3] L. Carroll, M. Sternitzke, B. Derby, Silicon carbide particle size effects in alumina-based nanocomposites, Acta Mater. 44 (11) (1996) 4543–4552.
[4] C.C. Anya, S.G. Roberts, Pressureless sintering and elastic constants of Al_2O_3–SiC nanocomposites, J. Eur. Ceram. Soc. 17 (1997) 565–573.
[5] M. Sternitzke, Review: structural ceramic nanocomposites, J. Eur. Ceram. Soc. 17 (1997) 1061–1082.
[6] J. Perez-Rigueiro, J.Y. Pastor, J. Llorca, E. Elices, P. Miranzo, J.S. Moya, Revisiting the mechanical behaviour of alumina/silicon carbide nanocomposites, Acta Mater. 46 (15) (1998) 5399–5411.
[7] T. Ohji, Y.-K. Jeong, Y.-H. Choa, K. Niihara, Strengthening and toughening mechanisms of ceramic nanocomposites, J. Am. Ceram. Soc. 81 (6) (1998) 1453–1460.
[8] L.P. Ferroni, G. Pezzotti, Evidence for bulk residual stress strengthening in Al_2O_3/SiC nanocomposites, J. Am. Ceram. Soc. 85 (8) (2002) 2033–2038.
[9] F.F. Lange, Powder processing science and technology for increased reliability, J. Am. Ceram. Soc. 72 (1) (1989) 3–15.
[10] L.C. Stearns, M.P. Harmer, Particle-inhibited grain growth in Al_2O_3–SiC: I. Experimental results, J. Am. Ceram. Soc. 79 (12) (1996) 3013–3019.
[11] J. Wang, S.Y. Lim, S.C. Ng, C.H. Chew, L.M. Gan, Dramatic effect of a small amount of MgO addition on the sintering of Al_2O_3–5 vol% SiC nanocomposite, Mater. Lett. 33 (1998) 273–277.
[12] Y.-K. Jeong, A. Nakahira, K. Niihara, Effects of additives on microstructure and properties of alumina–silicon carbide nanocomposites, J. Am. Ceram. Soc. 82 (12) (1996) 3609–3612.
[13] S.K.C. Pillai, B. Baron, M.J. Pomeroy, S. Hampshire, Effect of oxide dopants on densification, microstructure and mechanical properties of alumina–silicon carbide nanocomposite ceramics prepared by pressureless sintering, J. Eur. Ceram. Soc. 24 (2004) 3317–3326.
[14] A.M. Cock, I.P. Shapiro, R.I. Todd, S.G. Roberts, Effects of yttrium on the sintering and microstructure of alumina–silicon carbide nanocomposites, J. Am. Ceram. Soc. 88 (9) (2005) 2354–2361.
[15] K. Rundgren, O. Lyckfeldt, M. Sjöstedt, Improving powders with freeze granulation, Ceramic Ind. 4 (2003) 40–44.
[16] G.R. Anstis, P. Chantikul, B.R. Lawn, D.B. Marshall, A Critical evaluation of indentation techniques for measuring fracture toughness: 1. Direct crack measurements, J. Am. Ceram. Soc. 64 (9) (1981) 533–538.
[17] S. Gustafsson, Silicon carbide reinforced alumina and mullite ceramics, Ph.D. Thesis, Department of Applied Physics, Chalmers University of Technology, Gothenburg, Sweden, 2006, ISBN 91-7291-754-7.
[18] R.L. Coble, Sintering crystalline solids. II. Experimental test of diffusion models in powder compacts, J. Appl. Phys. 32 (5) (1961) 793–799.
[19] S.O. Bae, S. Baik, Critical concentration of MgO for the prevention of abnormal grain growth in alumina, J. Am. Ceram. Soc. 77 (10) (1994) 2499–2504.
[20] C.A. Bateman, S.J. Bennison, M.P. Harmer, Mechanism for the role of magnesia in the sintering of alumina containing small amounts of a liquid phase, J. Am. Ceram. Soc. 72 (7) (1989) 1241–1244.
[21] W.E. Kingery, H.K. Bowen, D.R. Uhlmann, Introduction to Ceramics, second ed., John Wiley & Sons, USA, 1976.
[22] F.F. Lange, Hot-pressing behaviour of silicon carbide powders with additions of aluminium oxide, J. Mater. Sci. 10 (1975) 314–420.
[23] I. Levin, W.D. Kaplan, D.G. Brandon, T. Wieder, Residual stresses in alumina–SiC nanocomposites, Acta Metall. Mater. 42 (4) (1994) 1147–1154.
[24] R.I. Todd, M.A.M. Bourke, C.E. Borsa, R.J. Brook, Neutron diffraction measurements of residual stresses in alumina/SiC nanocomposites, Acta Mater. 45 (4) (1997) 1791–1800.
[25] J. Fang, M.P. Harmer, H.M. Chan, Evaluation of subgrain formation in Al_2O_3–SiC nanocomposites, J. Mater. Sci. 32 (1997) 3427–3433.
[26] J. Luo, R. Stevens, The role of residual stress on the mechanical properties of Al_2O_3–5 vol% SiC nano-composites, J. Eur. Ceram. Soc. 17 (1997) 1565–1572.